Applied GIS

ISSN: 1832-5505
Vol-9 Issue-03 Aug 2021

Power Flow Control of UIPC Using Neural Networks in AC-DC Grid Connected Hybrid Micro grids

A RAMESH
ASSISTANT PROFESSOR
andalaramesh@gmail.com
D SHEKSHAVALI
ASSISTANT PROFESSOR
shaiksha456@gmail.com
B ARUNA
ASSISTANT PROFESSOR
bonasiaruna@gmail.com
Department of Electrical and Electronics Engineering, Sri Venkateswara Institute of Technology, N.H 44, Hampapuram, Rapthadu, Anantapuramu, Andhra Pradesh 515722

Abstract:
An alternative approach to controlling the power flow of linked AC-DC microgrids in framework-associated mixed microgrids, based on the implementation of a modified combined interphase power regulator (UIPC), is presented in this research. The framework that is being explored is a half-breed microgrid that is normally associated with matrices and consists of one AC microgrid and one DC microgrid. Interconnecting these microgrids using an altered UIPC is preferable than using the same related power converters. This paper's main contribution is an adaptation of the conventional UIPC architecture that reduces the number of intensity converters used for power exchange regulation across AC-DC microgrids from three per stage to two. A line power converter (LPC) and a transport power converter (BPC) are two force converters that the revised design keeps in mind; the former controls the DC transport voltage and the latter remembers one for each stage. Through the LPCs, the DC transports of the AC microgrid are linked to the main network, allowing it to operate in either capacitance mode (CM) or inductance mode (IM). The LPCs' control architecture makes use of a fluffy rationale regulator. The H∞ sifting approach is used by the fluffy derivation framework to reduce errors in the enrollment capacity structure. The DC microgrid supplies the LPCs with voltage via the BPC. Whatever the situation may be, the LPCs' DC interface voltage varies since a PV framework provides the DC microgrid power in this scenario. Hence, for DC side control of the BPC, another nonlinear unsettling influence observer based robust varied surface sliding mode control (NDO-MS-SMC) approach is presented as the following commitment to settle the DC connect variances. You may also use Neural to test the system's reaction.
Network controller in lieu of current fuzzy controller. The simulation findings validate the suggested power stream control method of the enhanced UIPC for mixed microgrids as adequate.

INTRODUCTION

In the last decade, DC microgrids have allowed DC power assets like photovoltaic (PV) systems, energy storage systems, and newly introduced DC loads like programmable DC electronic loads to become a part of the standard power grid [1]. In contrast, AC microgrids allow for the connection of alternating current (AC) power assets like wind turbines and AC loads like electrical engines to the power grids [2-3]. Eventually, smart networks will coordinate AC and DC microgrids, which include both sources of electricity and loads, as a hybrid architecture known as half breed microgrids [4]. Power converters really link the alternating current and direct current microgrids. Because of their partnership, microgrids may exchange electricity with one another as needed. If you want to trade a higher amount of intensity and increase consistent quality, you need generally connect the force converters in similar fashion [5]. Standard, matrix-associated half-breed microgrid architecture is shown in Fig. 1. Here we can see how the DC microgrid may take on the conventional DC transport-related loads, such as PV frameworks and ESSs [6]. Wind turbines, diesel generators, and the AC loads connected with conventional AC transportation could be part of the AC microgrid [7]. Either the force framework or a distinct entity might link the whole half-microgrid [8]. Figure 1 shows that two microgrids' fundamental transports (joins) are linked by equal related bidirectional connections. interlink power converters, which are force converters [9]. However, as shown below [8-17], there are a number of specific challenges associated with modelling power converters in crossover microgrids: - Microgrids possess a wide range of

ISSN: 1832-5505
Vol-9 Issue-03 Aug 2021

distinctive characteristics, such as exceptional voltage levels, stages, recurrence, and force changes.- Multiple microgrids may be combined to form a mixed microgrid. Think about it: three microgrids—two alternating current and one direct current. To avoid current flowing between equal associated ILCs in such a complex arrangement, the voltage greatness and period of the microgrids' basic transports must be equal, making it difficult and confusing to use equal associated ILCs to trade power between microgrids. It is essential that the transferred force between microgrids be uniformly distributed across all related ILCs with the same force ratings. System boundary changes (e.g., line impedance, load variety, etc.) affect the force sharing performance of identically connected ILCs. The shortfall is a nonlinear phenomenon, therefore if a microgrid fault occurs, the deficiency current may be divided inconsistently across ILCs. In this case, the power that is exchanged can drop significantly because the current that is flowing through the force converters is expected to exceed the apparent current limitations of the converters. As a result, this can cause microgrid vulnerability or load concealment.

- Microgrids experience oscillations in exchanged power and many uncertainties in produced power due to the intermittent behaviour of some distributed generation (DG) units. - Harmonics and other AC microgrid distortions generate a voltage loss due to the phase difference between individual load centres (ILCs) [15].
- The power factors in which the interconnected ILCs function could vary. Because of this, power and voltage fluctuations occur, which impacts the efficiency of power sharing.

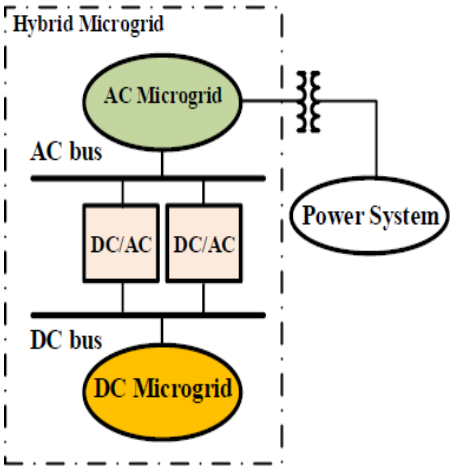

Fig.1.Atypicalgrid-connectedhybrid microgrid

Many written procedures and control mechanisms have been suggested to address the concerns outlined before. An equal-associated bidirectional ILC control system with several levels is suggested in [12]. With no consistent terminology across tomahawks and a consonant review, the control strategy's base has been set in a fixed reference outline (SRF). Being pre-structured in the SRF makes this method easy to implement, which is a major plus. In [13], a method for multi-level control based on hang control is suggested, with a hang plot used at the major control level. The proportional-resonant (PR) regulator was used on the AC side, whereas the comparable essential (PI) regulators were implemented on the DC side. The second level of control has modified the wave that was generated by the first level of control, and the third level is used to connect the utility to the crossover microgrid. A weakness-protected dynamic force control scheme for crossover microgrids connected to networks is suggested in [14]. To differentiate between dynamic and receptive force movements, the method has made use of an adjustable scalar. The authors of [15] demonstrated that force vacillations result from voltage imbalance. A method for controlling ILCs that are linked in parallel has been suggested; this method involves regulating the current through each force converter in order to modify the total flow through all of the ILCs. In light of this, a higher-rated ILC has been deemed "excess" for this purpose. The control plan becomes costly as a result of this. Also, the strategy can't lessen the responding force movements, and the suggested method can't stop consonant bending. In order to govern the distribution of power between two equal related inverters, a robust control plot has been designed in [16]. The present regulator of this method has been organised using the μ union examination.

inverters of power. To facilitate power sharing between two inverters linked in parallel, an optimal fragmented request regulator has been designed in [17]. Researchers in [18] have provided a blueprint for hybrid microgrids that adheres to IEEE 1547.4-2011. As shown in [19], a decentralised and self-advanced control architecture for limited microgrids is possible. Neighbourhood control actions without correspondence joins have been provided by the control strategy, strengthening the plan.

ISSN: 1832-5505
Vol-9 Issue-03 Aug 2021

Additionally, devices from the Flexible AC Transmission System (FACTS) have been used to regulate power flow in AC transmission systems. In this study, we learn how to use UIPC as a basic framework in a hybrid microgrid to regulate the traded power across different microgrids. Many force control applications with different control schemes have made use of the Realities devices. To improve voltage stability, the coupled force stream regulator (UPFC) has been used in [20]. Furthermore, the optimal UPFC fraction has been determined via genetic algorithms. In [21], the optimum regulation of the moving force in a transmission line was achieved using the between line power stream regulator (IPFC). In order to strengthen the force framework security via financial research, the authors of [22] have implemented the static VAr compensators (SVCs). A transmission line that links two territories in a force framework has the static simultaneous arrangement compensator (SSSC) applied to it [23]. In a power-sharing arrangement between two regions, the SSSC has proven convincing. The UIPC was first introduced in [24]. In place of stage-moving transformers in each stage, this improved version of the traditional IPC (interphase power regulator) makes use of force converters. According to [24], the UIPC is sufficient for controlling power streams. For the purpose of controlling the traded power across microgrids as the main network in a mixed microgrid scenario, this article zeroes in on small-scale changed UIPC. The main objectives of this project are: A half-and-half microgrid's core network and power may be managed with the use of the UIPC, as opposed to the use of equal related power converters, which have several control concerns [8–17]. In order to reduce the number of intensity converters used for power exchange regulation across AC-DC microgrids, the standard architecture of UIPC—which employs three force converters in each stage—is modified. An additional NDO-MS-SMC-based control method is presented for the DC side control of the BPC, and the problem of controlling the UIPC with a DC microgrid and its DC transport is addressed in this work, since the microgrid components in a cross-breed microgrid are not identical to those in an ordinary force framework. Consequently, this study focuses on UIPC as an alternative solution for controlling the flow of power across many microgrids in hybrid microgrids. The following are some advantages that the UIPC have over the conventional equal associated power converters: - Managing the power exchanged across microgrids without imposing cumbersome restrictions, such as same voltage extents, stages, etc., that are often required to connect the ILCs in a fair manner. - AAccording to [24], the UIPC can definitely limit the fault current without using an excess force converter, as shown in [15]. The addition of this component makes the connection more reliable, fairly priced, and simpler compared to control approaches like the rapid force control plot, which have traditionally been used for similarly linked ILCs.
The suggested modified UIPC provides a voltage confinement feature, as shown in [24], even though there are equal linked ILCs that provide direct electrical links amongst microgrids. The UIPC has the same ability to regulate the DC transport voltage of a DC microgrid as it does for an AC microgrid. The standard equal related ILCs were not used to grant this trademark. Therefore, in this study, a modified version of the UIPC is used to link half and half microgrids, achieving all the previously described characteristics. What follows is the structure of the rest of this work: The revised UIPC is shown in Section II. In the third section, we see an alternative method for determining the fluctuations in the regular DC transport voltage of the modified UIPC that relies on eyewitness testimony and is capable of controlling a strong surface sliding mode. Section IV displays the findings of the contextual analysis and reproductions. At last, the task is completed with Section V.

I. PROPOSED UIPC BASED STRUCTURE OF HYBRID MICROGRID AND DYNAMIC MODELING

Here we outline the UIPC-centric hybrid microgrid topology that has been suggested. This part also presents the dynamic model of the redesigned UIPC. Figure 2 shows the hybrid microgrid that was investigated. One alternating current (AC) microgrid and one direct current (DC) microgrid are linked via the user interface power control (UIPC) in the grid-connected hybrid microgrid. A diesel generator and associated AC and DC loads make up the AC microgrid. In the DC microgrid, you may find a PV system, a battery, and both AC and DC loads. A common DC bus, often called a DC link, connects the loads, PV system, while batteries.

ISSN: 1832-5505
Vol-9 Issue-03 Aug 2021

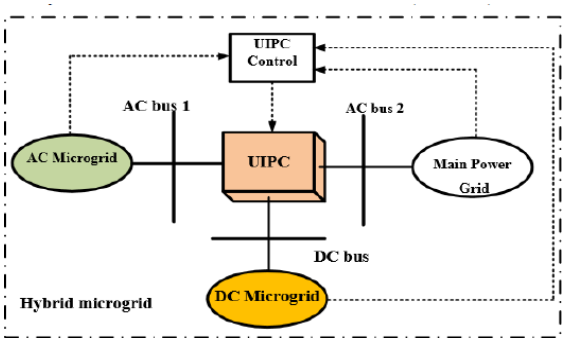

Fig. 2. Interconnection of AC-DC microgrids in grid-connected hybrid microgrid using UIPC

A. ConventionalUIPC

he UIPC's per-phase model is shown in Figure 3 and detailed in [24]. Voltage source converters (VSCs) replaced the interphase power regulator's (IPC) phase-moving transformers in this setup. Consequently, at each stage, three VSCs—VSC1, VSC2, and VSC3—are used to connect two AC transports, such as..1 and..2. The first two, VSC1 and VSC2, function as stage-moving converters, while the third, VSC3, controls the voltage. The arrangement voltage is inferred to the line via transformer T1 by VSC1, which operates in inductive mode. Transformer T2 is responsible for transferring the arrangement voltage to the line while VSC2 is operating in capacitive mode. One of the AC transports—in this case,..1—is linked to the third VSC, for instance VSC3, which regulates the AC voltage via transformer T3. An identical capacitor supplies the DC transport for each of the VSCs. That is how the dynamic forces of every VSC are provided by the DC connect voltage..... Consequently, the exchanged power between the two AC transports may be adjusted using stage edge control of VSC1 and VSC2. For further nuance, see [24].

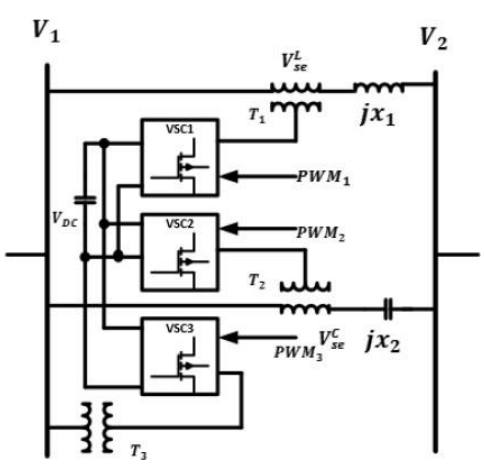

$$V_{se} = K_A V_{DC} \angle K_P \varphi_{se}$$

Fig. 3. Conventional structure of UIPC; each phase implements three power converters [24]

B. ProposedstructureofUIPC

We will start by making some changes to the traditional UIPC topology that we discussed in the last section. The next portion will then display the control plan of the updated UIPC. Here are several drawbacks of the traditional UIPC structure, as seen in Figure 3:
- Given that three VSCs are implemented in each phase, connecting three phases of AC buses requires nine VCSs, in addition to nine power transformers, which significantly increases the topology's cost. -All of the VSCs in a given phase have their DC connections linked in tandem. Nevertheless, as mentioned in [12, 25], VSCs that share DC connections have a tendency to cause oscillations in the common DC link voltage in response to changes in the VSCs' output powers or disturbances in the system model, such as changes to system parameters. When VSCs share a DC connection, voltage fluctuations in that link pose a serious threat. This issue is not addressed in reference [24].

Figure 4 shows the suggested improved UIPC model that aims to overcome the aforementioned obstacles. You can see that there is only one power converter used by each phase, denoted as $aPab$, where $b\in\{1,2,3\}$ represents the line number. The series voltage $Xbea\prod\varphi be=Xbef+aXbei$ is supplied to each line by these power converters via transformers Tb. Here, $Xbef$ and $Xbei$ are the real and imaginary portions of the injected series voltage, respectively. The equation for the line impedance is $Z\mathbf{O}b=R\mathbf{O}b+ba\mathbf{O}r$. The following is a broad outline of the controlled voltage source that the injected series voltage typically is:

ISSN: 1832-5505
Vol-9 Issue-03 Aug 2021

where $\mathbf{N}A$ represents the phase coefficient and $\mathbf{N}o$ the voltage amplitude. The PWM technique does affect the voltage amplitude coefficient KA, which is ±1, while the phase coefficient KP is typically equal to $\sigma 2$ and φye is τ. The injected voltage phase angle would coordinate the anti-parallel thyristor switches $S1$ and $S2$, which are controlled by the system. Depending on the sign of the phase angle, only one of these switches conducts at each phase at any given moment. The UIPC enters the inductive mode (IM) when the voltage phase coefficient KP equals +1, and $S1$ is turned on and $S2$ is turned off. Thus, when the phase coefficient The UIPC is operating in capacitive mode (CM) with $\boldsymbol{W}P$ equal to -1, and $S1$ is disabled while $S2$ is enabled. Hence, the controllability of the power transferred between the two AC buses, $X1$ and $V2$, is possible. Additionally, you can see that all phases in Fig. 4 have a single BPC. After that, the DC microgrid is linked to the DC bus of this BPC. In order to control the AC voltage and provide power to the DC microgrid, the BPC is linked to one of the AC buses (a weaker AC bus, also known as the AC microgrid bus) via transformer $TBP\mathbf{O}$. In this case, it is $X1$. Figure 5 shows a vector representation of the system voltages taking into account the injected voltage of the proposed UIPC. This graphic suggests that one may get;

$$\varphi_{se}^{L} = \varphi_1 + \alpha_1$$
$$\varphi_{se}^{C} = \varphi_2 + \alpha_2$$

These angles are calculated by considering different operation modes of the UIPC, i.e. IM or CM. In Equations (2)-(3), $\varphi seL$and $\varphi seC$are the phase angle of the voltage at the middle point of the transmission line, when the UIPC operates in IM and CM modes, respectively.
According to complex power flow concept [26], the exchanged power between the two AC buses would be determined as follows:

$$S = V_2\left(\frac{V_1 - V_2}{Z_L}\right)^* = (V_2\cos\delta_2 + jV_2\sin\delta_2)\frac{(V_1\cos\delta_1 + jV_1\sin\delta_1 - V_2\cos\delta_2 - jV_2\sin\delta_2)^*}{R_{L1} - jX_{L1}} \quad (4)$$

where,$\delta 1$and$\delta 2$arethephaseanglesofthevoltages
$V1$ and $V2$, respectively. After some mathematical manipulations, Equation (4) can be written asfollows:

$$P = \frac{R_{L1}V_1V_2(\cos\delta_1\cos\delta_2 + \sin\delta_1\sin\delta_2 + R_{L1}V_2^2) - X_{L1}V_1V_2(\cos\delta_1\sin\delta_2 - \sin\delta_1\cos\delta_2)}{{R_{L1}}^2 + {X_{L1}}^2} \quad (5)$$

$$Q = \frac{R_{L1}V_1V_2(\cos\delta_1\sin\delta_2 - \sin\delta_1\cos\delta_2) + X_{L1}V_1V_2(\cos\delta_1\cos\delta_2 + \sin\delta_1\sin\delta_2 + X_{L1}V_2^2)}{{R_{L1}}^2 + {X_{L1}}^2} \quad (6)$$

Inmicrogrids,$L1 \gg XL1$andweget:

$$P = \frac{V_1V_2(\cos\delta_1\cos\delta_2 + \sin\delta_1\sin\delta_2 + R_{L1}V_2^2)}{R_{L1}} = \frac{V_1V_2}{R_{L1}}(\cos(\delta_1 - \delta_2) + R_{L1}V_2^2) \quad (7)$$

$$Q = \frac{V_1V_2(\cos\delta_1\sin\delta_2 - \sin\delta_1\cos\delta_2)}{R_{L1}} = \frac{V_1V_2}{R_{L1}}\sin(\delta_2 - \delta_1) \quad (8)$$

Thus, the transferred active power is controlled bythe voltage magnitudes of the AC buses whereas the reactive power is controlled by the phase angle difference. The voltage magnitude and phase angle difference are controlled by the proposed UIPC implying that the exchanged active and reactive powers between two AC buses would be controlled easily. Considering Fig. 6, to evaluate the effects of theinjectedvoltage oftheUIPC,andusingKirchhoff Voltage Law, we obtain:

ISSN: 1832-5505
Vol-9 Issue-03 Aug 2021

$$V_1\angle\delta_1 - V_2\angle\delta_2 = (R_{L1} + jX_{L1})I + V_{se}\angle\varphi_{se} \quad (9)$$
$$= (R_{L1} + jX_{L1})\frac{P-jQ}{V_2^r - jV_2^i} + \left(V_{se}^r + jV_{se}^i\right) =$$
$$\left(\frac{V_2^r(R_{L1}P+X_{L1}Q)+(X_{L1}P-R_{L1}Q)}{(V_2^r)^2+\left(V_2^i\right)^2} + V_{se}^r\right)$$
$$+j\left(\frac{V_2^r(X_{L1}P-R_{L1}Q)+(R_{L1}P+X_{L1}Q)}{(V_2^r)^2+\left(V_2^i\right)^2} + V_{se}^i\right)$$

Inthemicrogrids,$L1P \cong RL1Q$andweget:

$$V_1\angle\delta_1 - V_2\angle\delta_2 = \left(\frac{V_2^r(R_{L1}P+X_{L1}Q)}{\left(V_2^r\right)^2+\left(V_2^i\right)^2} + V_{se}^r\right) + jV_{se}^i \quad (10)$$

Also,$L1P \gg XL1Q$andwehave:

$$V_1\angle\delta_1 - V_2\angle\delta_2 = \left(\frac{V_2^r + V_{se}^r\left(\left(V_2^r\right)^2+\left(V_2^i\right)^2\right)}{\left(V_2^r\right)^2+\left(V_2^i\right)^2}\right) + jV_{se}^i \quad (11)$$

The exchanged power between the DC link and the AC link (..1) can be obtained using the power balance equation as follows:

$$V_{DC}I_{DC}^{UIPC} = \frac{3}{2}V_1^d i_1^d$$

where $IDCUIPC$is the current flowing in the DC link of the UIPC, and $V1d$ and $i1d$ are the d-axes voltage and current of the AC link, respectively.

ISSN: 1832-5505
Vol-9 Issue-03 Aug 2021

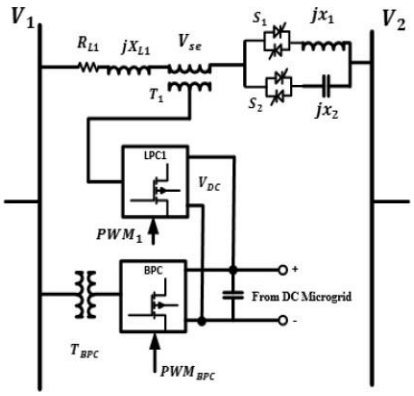

Fig. 4. Proposed topology of UIPC (each phase implements only one power converter, named asLPC)

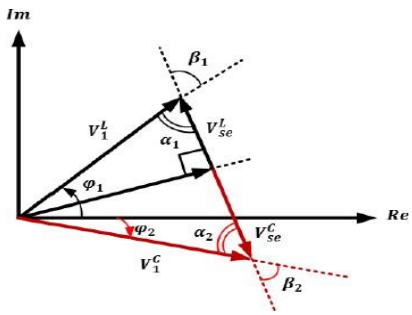

Fig.5.VoltageswhentheproposedUIPCisinvolved

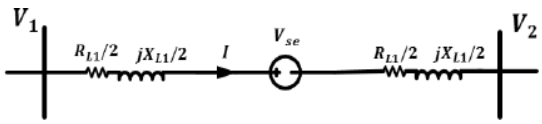

Fig. 6. Model of each phase of system considering injected voltage of proposed UIPC

Figure 7 shows the per-stage geographical layout of the cross-breed microgrid's planned UIPC-based linked microgrids. This picture also shows the overall control structure of the UIPC that has been suggested. Both series VSC control and DC connect control based on NDO-MS-SMC are components of the control framework. A structure that utilises an ideal H∞ based fuzzy reasoning regulator is employed by the Series VSC regulate subsystem to regulate the injected voltage and switches $S1$ and $S2$. You may see this control subsystem in the section that follows. The SMC-based DC connect Control subsystem relies on another annoyance spectator-based robust multi-surface sliding mode control mechanism to stabilise the typical DC interface voltage fluctuations. What follows is a representation of this control structure method.

Fig.7. A per-phase model of the UIPC and UIPC control system interconnecting AC-DC microgrids The suggested UIPC geography provides the following advantages over the conventional layout: - Each stage requires just one LPC.

In the three-stage setup, only one BPC is needed. Accordingly, three force transformers and four VSCs are required by the generic model.
- AIt is the DC microgrid that supplies the DC interface voltage. The ability to link the AC and DC microgrids is granted to the UIPC via this component.
- AThe LPCs' control structure makes use of an ideal fluffy reasoning regulator, which reduces the number of errors.

ProposedcontrolstrategyforLPCs

Fig. 7 shows that the proposed UIPC control scheme has two subsystems: the LPCs control approach and the SMC based control plan for the BPC. There are control cooperations in these control subsystems as well. The suggested method of control for each LPC at each step is shown in Figure 8. It seems that the line current and the injected arrangement voltage have been approximated and scaled. The next step is to use a bandpass channel to extract the important components of these scaled signals. We use MATLAB [27] to resolve the channel's boundaries, which entails the following steps: - As shown in the following segment, we use an unsettling influence eyewitness based powerful different surface sliding mode control technique to dampen the voltage fluctuations of the DC interface.

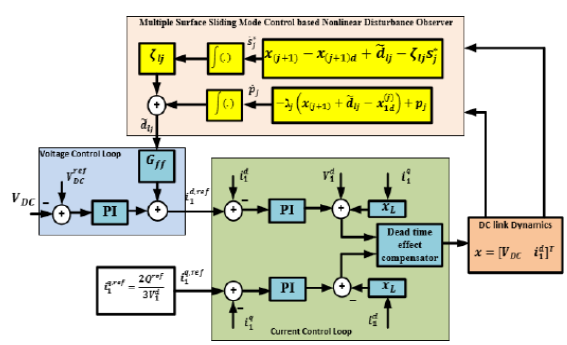

$$T_f = \frac{190.10s}{s^2+190.10s+145321}$$

ISSN: 1832-5505
Vol-9 Issue-03 Aug 2021

After that, we may calculate the filtered signals' rms values. The best fuzzy logic controller (FLC) that was suggested receives the injected voltage mistake. A PLL is used to measure the phase of the injected voltage. Next, we get the phase's sign, which is actually KP in Equation (1). From this sign, we may deduce that the UIPC runs in either IM or CM mode. Consequently, the correct phase shift is used; $+\pi 2$ for IM mode and $-\pi 2$ for CM mode. In addition, the operating modes determine whether the switches $S1$ and $S2$ are active or disabled. The authors of this study have thoroughly defined and confirmed the H∞ filtering design technique in [28], which is used to build the optimum FLC. The control system of all LPCs receives a DC li gure 8 gnal. H gnal (1 The in sted a WM s

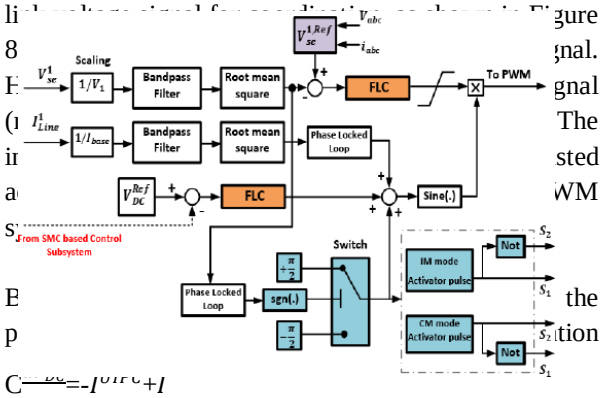

B the p tion

C=-I+I

Fig.8.ProposedcontrolstrategyforLPCs

II. PROPOSED NDO MULTIPLE SURFACE SMC BASEDDCLINKVOLTAGECONTROLOFUIPC

The DC links of the LPC and BPC are in parallel and connected to the common DC bus of the DC microgrid. As mentioned before, the DC link voltage would be unstable due to the output active power change of power converters, loads or PV system in the DC microgrid. Thus, a new NDO-MS-SMC is usedinthissectiontocontroltheDClinkvoltageof theproposedUIPC.

A.Structureofproposedcontrolscheme

Fig.9showstheproposedcontrolschemeforBPC.

In fact, and as described earlier, the BPC is responsible to regulate the DC link and therefore, the proposedNDO-MS-SMCstrategyisappliedtothe circuit 3-the NDO and 2-the present control loop. The DC microgrid's uncertainty and power changes are estimated by the NDO. As an added bonus, the NDO supplies the current control loop and the dead-time compensation unit with a reference signal. The voltage control loop uses feedforward power disturbance in conjunction with optimum proportional-integral (PI) controllers to make up for the constitutional delay embedded in the dynamics of the current control loop and the suggested disturbance observer. The genetic algorithm (GA) is used to fine-tune the PI controllers in the current and voltage control loops.

Fig. 9. Control of DC link of BPC based on new NDO-MS-SMC strategy

B.Dynamicmodelofnominalsystem

Firstly, the dynamic equations of the common DC link of BPC will be extracted without using any parametric uncertainty; so called the nominal model. Using Kirchhoff Current Law we get:

$$dt \quad DC \quad dist \qquad (14)$$

where, C is the capacitor of the common DC link,and $Idist=IDCPV+IESS+IL$ is the disturbancecurrent in which $IDCPV$ is the output DC current of the PV system, $IESS$ is the energy storage system (ESS) current (for example, a battery), and IL is the lumped DC loads current.

The BPC model in dq-frame can be expressed as follows [29]:

$$\begin{cases} V_o^d = \left(\frac{di^d}{dt}\right) + \omega L i^q + i^d R \\ V_o^q = \left(\frac{di^q}{dt}\right) - \omega L i^d + i^q R \end{cases} \qquad (15)$$

ISSN: 1832-5505
Vol-9 Issue-03 Aug 2021

Where, $Vo$and $V1$ are the output AC voltage of the BPC and AC bus to which the BPC is connected, respectively, ω is the angular frequency in rad/s, and L and R are the inductance and resistance of the output filter of the BPC, respectively.
Therefore, using Equations (12), (14), and (15) we obtain:

$$\begin{cases} \frac{dV_{DC}}{dt} = -\frac{3V_1^d i_1^d}{2CV_{DC}} + \frac{1}{C} I_{dist} \\ \frac{di_1^d}{dt} = \frac{V_0^d - V_1^d}{L} - \omega i_1^q - \frac{R}{L} i_1^d \end{cases}$$

Equation (17) indicates a system with nonlinear terms. This is the nominal model of the system.

C.Dynamicmodelofperturbedsystem

The uncertainties are considered on the capacitanceof the DC link C, the disturbance current , and the inductance L as follows:

$$\frac{1}{C} = \frac{1}{\bar{C}(1+\rho_C\theta_C)} = \frac{1}{\bar{C}} - \frac{\rho_C}{\bar{C}}\theta_C(1+\rho_C\theta_C)^{-1} \quad (18)$$

$$\frac{1}{L} = \frac{1}{\bar{L}(1+\rho_L\theta_L)} = \frac{1}{\bar{L}} - \frac{\rho_L}{\bar{L}}\theta_L(1+\rho_L\theta_L)^{-1} \quad (19)$$

$$I_{dist} = \bar{I}_{dist}\left(1+\rho_{I_{dist}}\theta_{I_{dist}}\right) \quad (20)$$

where,$\bar{C}$,$\bar{L}$,and$\bar{I}dist$ arethenominalvaluesofC,L, and$Idist$,respectively,andρC,ρL,and$\rho Idist$and θC, θL, and $\theta Idist$represent the probable perturbations on these parameters which are random numbers in the range of -1 to +1.

Introducing these perturbed parameters into the nominal system (17) we get:

$$\begin{aligned} \dot{x_1} &= \left(\frac{1}{\bar{C}} - \frac{\rho_C}{\bar{C}}\theta_C(1+\rho_C\theta_C)^{-1}\right)\left(-\frac{3V_1^d x_2}{2x_1}\right) \\ &+ \left(\frac{1}{\bar{C}} - \frac{\rho_C}{\bar{C}}\theta_C(1+\rho_C\theta_C)^{-1}\right)\left(\bar{I}_{dist}\left(1+\rho_{I_{dist}}\theta_{I_{dist}}\right)\right) \quad (21) \\ &= -\frac{3V_1^d x_2}{2\bar{C}x_1} + \frac{\bar{I}_{dist}}{\bar{C}} + \left(\frac{3V_1^d x_2}{2x_1}\right)\rho_C\theta_C(1+\rho_C\theta_C)^{-1} + \\ &\frac{\bar{I}_{dist}}{\bar{C}}\rho_{I_{dist}}\theta_{I_{dist}} - \frac{\bar{I}_{dist}}{\bar{C}}\rho_C\theta_C(1+\rho_C\theta_C)^{-1}\left(1+\rho_{I_{dist}}\theta_{I_{dist}}\right) \end{aligned}$$

$$\begin{aligned} \dot{x_2} &= \left(\frac{1}{\bar{L}} - \frac{\rho_L}{\bar{L}}\theta_L(1+\rho_L L)^{-1}\right)\left(-Rx_2 + u - V_1^d\right) - \omega i_1^q \quad (22) \\ &= \frac{R}{\bar{L}}x_2 + \frac{u}{\bar{L}} - \frac{V_1^d}{\bar{L}} - \omega i_1^q + \frac{\rho_L\theta_L}{\bar{L}}(Rx_2 - u + V_1^d)(1+\rho_L\theta_L)^{-1} \end{aligned}$$

D.DesignofNDO-MS-SMC

In this subsection, the proposed NDO-MS-SMC, indicated in Fig. 9, is designed by pursuing the following steps:

Step 1. Determine the perturbed system model as the standardform:Todothis,Equations(21)and(22) should be rewritten using the following disturbance parameters:

$$\begin{aligned} d_1(x,t) &= \frac{\bar{I}_{dist}}{\bar{C}} + \left(\frac{3V_1^d x_2}{2x_1}\right)\rho_C\theta_C(1+\rho_C\theta_C)^{-1} + \\ &\frac{\bar{I}_{dist}}{\bar{C}}\rho_{I_{dist}}\theta_{I_{dist}} - \frac{\bar{I}_{dist}}{\bar{C}}\rho_C\theta_C(1+\rho_C\theta_C)^{-1}\left(1+\rho_{I_{dist}}\theta_{I_{dist}}\right) \quad (23) \\ d_2(x,u,t) &= -\omega i_1^q + \frac{\rho_L\theta_L}{\bar{L}}(Rx_2 - u + V_1^d)(1+\rho_L\theta_L)^{-1} \quad (24) \end{aligned}$$

$d1(x,t)$isnamedasmatcheduncertaintywhereas $d2(x,u,t)$ is unmatched uncertainty, according to nonlinear control terminology [30]. Thus, the system is written in the following general standard form:

$$\dot{x}_n = a(x,t) + b(x,t)u(t) + d_n(x,u,t)$$

where,b=1$\bar{L}$.Thedisturbancein(25)iscontinuous

Step 2. Define the multiple surface sliding surfaces,as follows [30]:

$$s_j^* = s_j - s_j(0)e^{-\beta_j t}$$

$$s_j = x_j - x_{jd}$$

where, β is a positive constant value and xjd is the desired state trajectories. The purpose is to enforce each sliding surface $sj*$ to zero such that $xj \cong xjd$. Therefore, obtaining the derivative of the first sliding surfaces we have:

$$\dot{s}_1^* = \dot{s}_1 + s_1(0)\beta_1 e^{-\beta_1 t} = s_2 + x_{2d} + d_{l1} - \dot{x}_{1d}$$

Theestimationerrorisdefinedasfollows:

$$e_{d_{lj}} = d_{lj} - \tilde{d}_{lj}$$

Step 3. Design actual control law: Until now, the virtualcontrolinputsweredesigned;theyare$x1d$,$2d$. To stabilize the uncertain system (25), the following actual control input is proposed here as follows:

$$u = -\frac{1}{b(x,t)}\left(a(x,t) + \tilde{d}_{ln} - x_{1d}^{(n)} + \zeta_{ln}s_n^* + \zeta_s sat(s_n^*)\right)$$

Therefore;

$$u = -\bar{L}\left(a(x,t) + \tilde{d}_{l2} - \ddot{x}_{1d} + \zeta_{l2}s_2^* + \zeta_s sat(s_2^*)\right)$$

where, $\zeta l2$ is a linear gain, ζs is the switching gain and the hyperbolic tangent function is approximately equal to:

$$sat(s_2^*) = \begin{cases} sgn(s_2^*) & , \ if\ |s_2^*| > \varrho \\ \frac{s_2^*}{\varrho} & , \ if\ |s_2^*| \le \varrho \end{cases}$$

where,ϱisasmallpositiveconstant.Substituting (32)in(29),thedynamicsoftheslidingsurface$s2*$ is:

ISSN: 1832-5505
Vol-9 Issue-03 Aug 2021

$$\dot{s}_2^* = -\zeta_{l2} s_2^* - \zeta_s sat(s_2^*)$$

It should be noted that the discrete control component was not included in the obtained equations when getting the derivatives of the design procedure disturbances. The reason for this is because the control signal that is created when an SMC-based controller is developed has two components; one is the equivalent control energy aec, and the other is a discrete component that is added to the produced control signal to make it resistant to disturbances. It should be noted that the goal of the design process while creating the controller and taking disturbances into account is to derive the equivalent control energy law uec from the Lyapunov energy function. The produced signal is then made more robust by manually adding the discrete term bd to the control rule. Consequently, the design phase occurs when the control law's time derivative is real. Please see [33] for more information.

Step4.Obtainingthe disturbanceobserverdynamics: The NDO aims to estimates the disturbance $\tilde{d}li$ as follows:

$$\begin{cases} \tilde{d}_{lj} = p_j + \lambda_j s_j^* \\ \dot{p}_j = -\lambda_j \left(s_{(j+1)} + x_{(j+1)d} + \tilde{d}_{lj} - x_{1d}^{(j)} \right) \end{cases} \quad (35)$$

where, pj and λj are a dummy variable and gains of the observer, respectively. Calculating the derivative of $\tilde{d}\ lj$ we get:

$$\dot{\tilde{d}}_{lj}^{(1)} = \dot{p}_j + \lambda_j \dot{s}_j^* = -\lambda_j \left(s_{(j+1)} + x_{(j+1)d} + \tilde{d}_{lj} - x_{1d}^{(j)} \right) + \lambda_j \left(s_{(j+1)} + x_{(j+1)d} + d_{lj} - x_{1d}^{(j)} \right) = \lambda_j \left(d_{lj} - \tilde{d}_{lj} \right) = \lambda_j e_{d_{lj}} \quad (36)$$

and;

$$\|\dot{d}_l\| \le \gamma \quad (37)$$

Step 5. Stability proof: The Lyapunov function is defined as:

$$V_1(e_{d_l}) = e_{d_l}{}^T P e_{d_l}$$

Calculating the derivative of Lyapunov function and using Equations (34)-(36) we get:

$$\dot{V}_1 = e_{d_l}{}^T (D^T P + PD) e_{d_l} + 2 e_{d_l}{}^T P \dot{d}_l \le -e_{d_l}{}^T Q e_{d_l} + 2\|e_{d_l}\| . \|P\| . \|\dot{d}_l\|$$

where, $D = diag[\lambda \quad \lambda\ ]$ Q is a positive arbitrary matrix, and P is a positive matrix such that the following constraint is satisfied.

$$D^T P + PD = -Q \quad (40)$$

Analytically:

$$P = \begin{bmatrix} P_{11} & P_{12} \\ P_{12}^T & P_{22} \end{bmatrix} \quad (41)$$

and we have:

$$\begin{bmatrix} \lambda_1 & 0 \\ 0 & \lambda_2 \end{bmatrix} \begin{bmatrix} P_{11} & P_{12} \\ P_{12}^T & P_{22} \end{bmatrix} + \begin{bmatrix} P_{11} & P_{12} \\ P_{12}^T & P_{22} \end{bmatrix} \begin{bmatrix} \lambda_1 & 0 \\ 0 & \lambda_2 \end{bmatrix} = -Q \quad (42)$$

Therefore, considering Q as an identical matrix, and using (30) and (35)-(37), e_{d_l} will be bounded by;

$$\|e_{d_l}\| \le \lambda_l \quad (43)$$

where;

$$\lambda_l = \frac{2\|P\|\gamma}{\lambda_m} \quad (44)$$

and the system is robustly stable.

4.Neuralnetwork:

A neural network may be either a real-life circuit made up of real neurons or, more recently, an artificial neural network made up of fake neurons.[1] So, a neural network may be either an artificial network designed to solve AI issues or a biological network composed of actual neurons in the human body. The weights represent the connections of the real neuron. When the weight is positive, it indicates an excitatory link; when it is negative, it indicates an inhibitory one. We add up all the inputs after applying a weight to them. The term for this action is a linear combination. Activation functions are used to regulate the output amplitude in the end. As an example, the typical permissible range of output is from 0 to 1, while it might also be between -1 and 1. Applications that allow for the training of artificial networks using datasets include predictive modelling and adaptive control. Networks are capable of self-learning via experience, drawing inferences from a complicated and apparently unconnected dataset.

.

ISSN: 1832-5505
Vol-9 Issue-03 Aug 2021

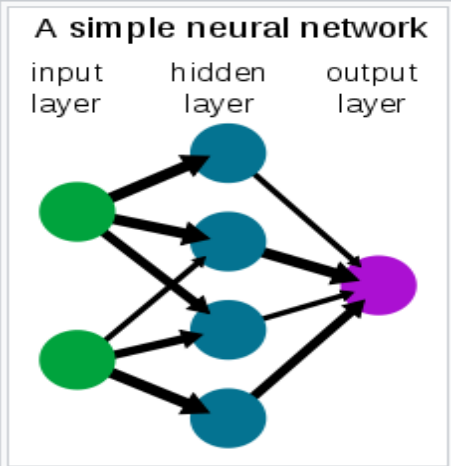

Simplified view of a feedforward artificial neural network

Artificialintelligence:

A neural network (NN), also known as an artificial neural system (ANN) or a mimicked neural network (SNN), is a network of real or artificial neurons that work together to process data using a scientific or computational model based on a connectionistic approach to computation. The topology of an ANN often varies depending on the inbound and outbound data that flows through the system, making it a very dynamic framework.

To put it more simply, neural networks are dynamic tools that present information in a non-linear fashion. They may be used to find patterns in data or to show complicated relationships between data sources and results.

Using the connections between the handling components and component borders, a system of simple preparing components (fake neurons) may demonstrate complicated global behaviour in a counterfeit neural network. The idea of fake neurons was first put out in 1943 by a rationalist and neurophysiologist working together at the University of Chicago, Warren McCulloch.

Repeated Hopfield organises are an example of a more traditional sort of artificial neural system.

Although he referred to them as "B-type chaotic machines" in his 1948 article Intelligent Machinery, Alan Turing seems to have been the first to suggest the concept of a neural network.

The ability to derive a capability from perceptions and then put it to use is where artificial neural system models really shine. Aside from supervised learning algorithms, unsupervised neural networks can learn representations of data that capture the unique properties of data acquisition (e.g., the Boltzmann machine, 1983) and, more recently, deep learning algorithms, which can demonstrably improve their proficiency with the data's dissemination capacity. When human planning of such capabilities is impractical due to the unpredictability of the data or task, neural network learning becomes invaluable.

Applications:

Many different domains may make use of neural networks. In most cases, the following categories will include the tasks that are often handled by fake neural networks:

• Relapse analysis, or function estimate, which includes time arrangement expectation and presentation.
• Categorization, which encompasses example and grouping identification, anomaly detection, and sequential tracking.

Sifting, grouping, dazzle signal partitioning, and pressure are all aspects of data processing. Nonlinear framework identification[19] and control (vehicle control, process control), game-playing and dynamic (backgammon, chess, dashing), design recognition (radar frameworks, face ID, object recognition), grouping recognition (motion, discourse, transcribed content recognition), clinical conclusion, financial applications, information mining (or information revelation in databases, "KDD"), perception, and email spam sifting are all areas where ANNs have found application. One example is the possibility of creating a semantic profile of the client's preferences using images that have been trained for object recognition.

Neuroscience:

A subfield of theoretical and computational neuroscience, this area studies and models natural brain networks in a hypothetical and computational setting. Given that neuronal frameworks are intrinsically linked to cognitive processes and actions,

the area is strongly linked to social and psychological performance.

Modelling natural neural frameworks to understand their operation is the main goal of the discipline. Researchers

ISSN: 1832-5505
Vol-9 Issue-03 Aug 2021

in the field of neuroscience try to piece together this knowledge by drawing connections between observed natural processes (information), biologically plausible tools for brain processing and learning (models of organic neural systems), and theories (such as the factual learning hypothesis and the data hypothesis).

Typesof models

We use a plethora of models, each with its own unique set of characteristics and representation of a different aspect of neural networks. Models of behaviour emerge from conceptual brain modules that communicate to final subsystems, progressing from models of the transitory conduct of individual neurons to models of the components of neural hardware resulting from cooperations between solitary neurons. These include models of the transient and long-term plasticity of neural networks, as well as their relationship to learning and memory at both the neuronal and network levels.

SIMULATIONRESULTS:

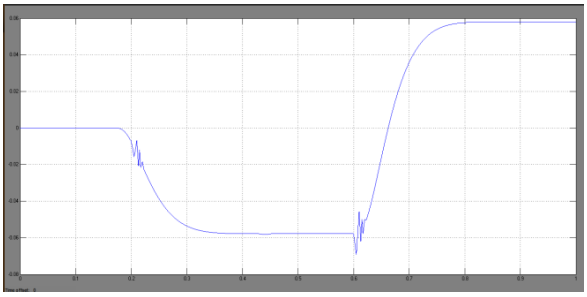

VSESeriesInjectedVoltage

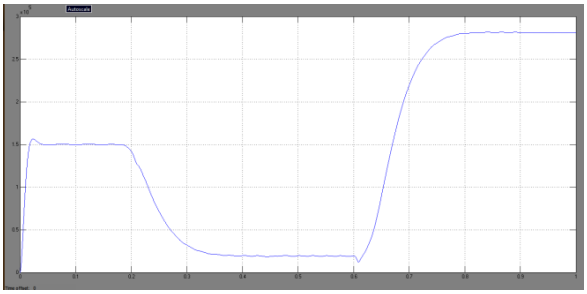

PseInjectedPower

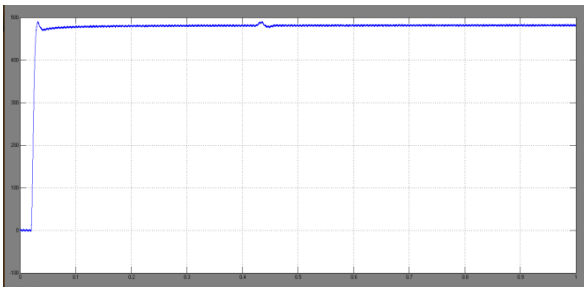

DcLINKVOLTAGE

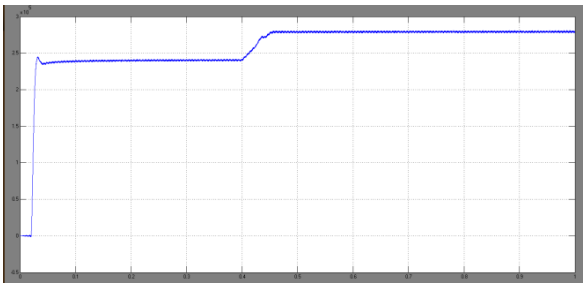

Fig.14.ActivepowerofDClinkwhen40kWis demanded from the AC side

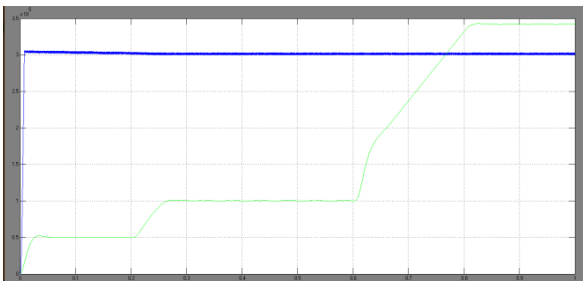

Fig.13.Generationineachmicrogrid

SimulationresultswithNeural NeworkController:

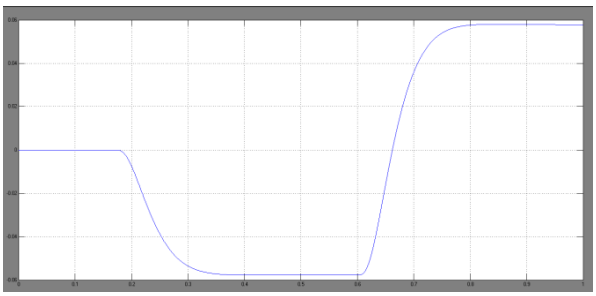

VSESeriesInjectedVoltage

ISSN: 1832-5505
Vol-9 Issue-03 Aug 2021

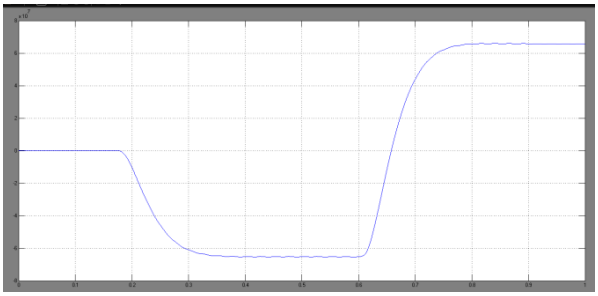

PseInjectedPower

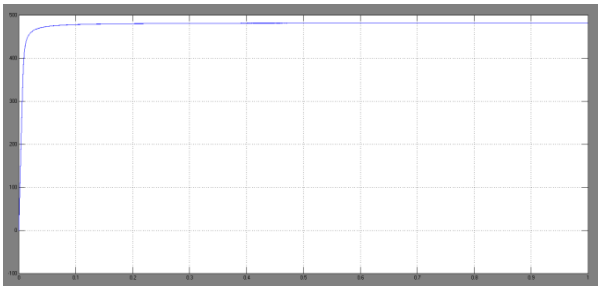

DcLINKVOLTAGE

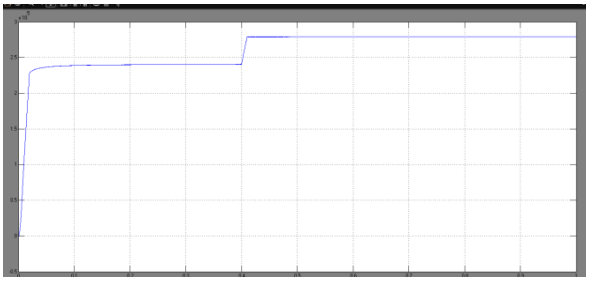

Fig.14.ActivepowerofDClinkwhen40kWis demanded from the AC side

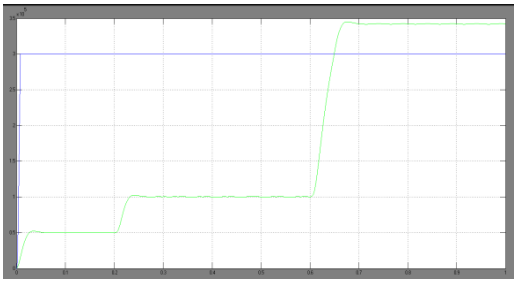

Fig.13.Generationineachmicrogrid

CONCLUSION:

Future smart grids are likely to use a hybrid microgrid structure to integrate the clean energy sources and both alternating current and direct current loads. Because it combines the best features of AC and DC microgrids, this setup is ideal. Interconnected AC and DC microgrids' power exchange control is a common issue with this design. Instead of using the problematic parallel-connected power converters, this research suggests a UIPC based solution. Initially, a revised UIPC architecture was suggested, and subsequently, efficient control mechanisms were implemented for this revised architecture. The simulation findings confirmed the accuracy of the updated model and the efficiency of the control system for power exchange between AC and DC microgrids. A Neural Network controller outperforms a fuzzy logic controller in terms of system performance.

VI.REFERENCES

[1] Runfan Zhang, Branislav Hredzak, "Distributed Finite-Time Multi-Agent Control for DC Microgrids with Time Delays", IEEE Transactions on Smart Grid, Early Access, 2018.

[2] Kumar Utkarsh, et al, "Distributed Model-predictiveReal-timeOptimalOperationofaNetwork of Smart Microgrids", IEEE Transactions on Smart Grid, Early Access, 2018.

[3] Haifeng Qiu, et al, " Bi-level Two-stage Robust Optimal Scheduling for AC/DC Hybrid Multi-microgrids", IEEETransactions on Smart Grid, Early Access, 2018.

[4] Pengfeng Lin, et al, "A Distributed Control Architecture for Global System Economic Operation in Autonomous Hybrid AC/DC Microgrids", IEEE Transactions on Smart Grid, Early Access, 2018.

[5] Daniel E. Olivares, et al, "Trends in Microgrid Control", IEEE Transactions on Smart Grid Volume: 5, Issue: 4, pp. 1905 – 1919, 2014.

[6] Jongwoo Choi, et al, "Robust Control of a Microgrid Energy Storage System using Various Approaches", IEEE Transactions on Smart Grid, Early Access, 2018.

[19] Huanhai Xin, et al., "A Decentralized Hierarchical Control Structure and Self-Optimizing Control Strategy for F-P Type DGs in Islanded Microgrids", IEEE Transactions on Smart Grid, Volume: 7, Issue: 1, pp. 3 – 5, 2016.

[20] Priyank Srivastava, Rashmi Pardhi "A Review onPowerSystemStabilityandApplicationsofFACT Devices"InternationalJournalofEngineering

ISSN: 1832-5505
Vol-9 Issue-03 Aug 2021

ResearchandApplications,Volume:3,Issue:3, pp.879-883, 2013.

[21] Akanksha Mishra and G.V. Nagesh Kumar, “Congestion Management of Power System with InterlinePowerFlowControllerUsingDisparityLine Utilization Factor and Multi-objective Differential Evolution”CSEEJournalof PowerandEnergySystems, Volume:1,Issue:3,pp.76-85 2015

[22] B. Vijay Kumar, et al., "Optimization of UPFC location and capacity to improve the stability using ABC and GSA algorithm", IEEE,PowerandEnergy ConferenceatIllinois(PECI),2015.

[23] K.K. Sen, "SSSC-static synchronous series compensator: theory, modeling, and application", IEEE Transactions on Power Delivery, Volume: 13, Issue: 1, pp. 241 - 246,1998.

[24] J. Pourhossein, et al., "Unified Interphase Power Controller(UIPC)ModelingandItsComparisonwith IPC and UIPFC", IEEE